Molecular Pseudo-Halogen Engineering Enables Remarkable Birefringence Enhancement in Hybrid Perovskites

Yao Yao,[1,3,4] Yanqiang Li,[1,2,*] Bin Chen,[1] Yipeng Song,[1,3,4] Weiqi Huang,[1,4] Zhiyong Bai,[1] Junhua Luo,[1,3,4,*] and Sangen Zhao[2,*]

[1]State Key Laboratory of Functional Crystals and Devices, Fujian Institute of Research on the Structure of Matter, Chinese Academy of Sciences, Fuzhou 350002, China

[2]Quantum Science Center of Guangdong-Hong Kong-Macao Greater Bay Area, Shenzhen 518045, China

[3]University of the Chinese Academy of Sciences, Beijing 100049, P.R. China

[4]Fujian College, University of Chinese Academy of Sciences, Fuzhou, Fujian 350002, China

EXPERIMENTAL PROCEDURES

Reagents: All the reagents including 1,4-dimethylpiperazine (Aladdin, 99%), HCl (Aladdin, 36.0−38.0%), potassium thiocyanate (KSCN, Aladdin, 99%), cadmium nitrate tetrahydrate ($Cd(NO_3)_2·4H_2O$, Aladdin, ACS), and cadmium chloride ($CdCl_2$, Aladdin, 99%) are purchased from commercial sources without further purification.

Synthesis: Colorless block crystals of $(C_6N_2H_{15})Cd(SCN)_3$ were obtained by slowly evaporating aqueous solutions (20 mL) containing $Cd(NO_3)_2·4H_2O$ (0.308 g, 1 mmol) and KSCN (0.388 g, 4 mmol) in 1,4-dimethylpiperazine (0.114 g, 1 mmol) and hydrochloric acid solution at room temperature for few days. Colorless plate crystals of $(C_6N_2H_{16})Cd_2Cl_6·2H_2O$ were obtained by slowly evaporating hydrochloric acid solutions (10 mL) containing $CdCl_2$ (0.55 g, 3 mmol) and 1,4-dimethylpiperazine (0.114 g, 1 mmol) at room temperature for few days.

Single-Crystal Structure Determination: High-quality colorless crystals of $(C_6N_2H_{15})Cd(SCN)_3$ and $(C_6N_2H_{16})Cd_2Cl_6·2H_2O$ were selected using an optical

microscope for single-crystal X-ray diffraction (XRD) analysis. The diffraction data were collected by using Mo Kα radiation (λ = 0.7107 Å) at 100 K on a Rigaku XtaLAB Synergy *R* diffractometer. The collection of the intensity data, cell refinement, and data reduction were carried out with the CrysAlisPro software. Using Olex2, the structure was solved with the SHELXS[1] structure solution program using Direct Methods and refined with the SHEXL[2] refinement package using Least Squares minimization. Final refinements include anisotropic displacement parameters. Both structures were verified by the ADDSYM algorithm from the program PLATON,[3] and no higher symmetry was found. Details of crystal parameters, data collection, and structure refinement were summarized in Table S1. The atomic coordinates and equivalent isotropic displacement parameters were listed in Table S2. The anisotropic displacement parameters were listed in Table S3. Selected bond lengths and bond angles were presented in Table S4 and Table S5.

Elemental Analysis and Scanning Electron Microscope Mapping: Semiquantitative microprobe analyses on the $(C_6N_2H_{15})Cd(SCN)_3$ and $(C_6N_2H_{16})Cd_2Cl_6{\cdot}2H_2O$ crystals were performed with the aid of a field emission scanning electron microscope (Nova NanoSEM 230) equipped with an energy-dispersive X-ray spectroscope (EDS). The energy dispersive spectra and elemental mapping were collected on visibly clean surfaces of the sample.

XPS Analysis: The X-ray photoelectron spectroscopy (XPS) was operated on the ESCALAB 250Xi XPS instrument by using Al Kα radiation as the source

Powder XRD: Powder XRD measurements for the samples of $(C_6N_2H_{15})Cd(SCN)_3$ and $(C_6N_2H_{16})Cd_2Cl_6{\cdot}2H_2O$ were carried out with a Miniflex 600 diffractometer equipped with an incident beam monochromator set of Cu Kα radiation (λ = 1.5418 Å). Data were collected over a 2θ range of 5-70° with a scan step width of 0.02° and a scanning rate of 2° min^{-1}.

FTIR Analysis: Fourier transform infrared spectroscopy (FTIR) of

$(C_6N_2H_{15})Cd(SCN)_3$ and $(C_6N_2H_{16})Cd_2Cl_6 \cdot 2H_2O$ in the wavenumber range of 4000-400 cm^{-1} were recorded on the Bruker Vertex 70 infrared spectrometer.

Raman Analysis: Raman spectroscopy of $(C_6N_2H_{15})Cd(SCN)_3$ and $(C_6N_2H_{16})Cd_2Cl_6 \cdot 2H_2O$ between 4000-400 cm^{-1} range were collected on a LabRAM HR Evolution Raman microscope (HORIBA Scientific) with a solid-state laser corresponding to the green light (λ = 532 nm).

Angle-resolved Polarized Raman Analysis: Raman measurements were performed using a double spectrometer (LabRAM Odyssey) equipped with a liquid nitrogen cooled CCD detector. A 532 nm laser (Excelsior, Spectra-Physics) was focused onto the sample with a 50× objective and a power of 10%. A polarizer was placed between the edge filter and the detector. The incident laser beam is polarized, and an analyzer was placed just before the spectrometer entrance, allowing the investigation of the scattered light polarization along directions parallel and perpendicular to the incident light polarization. Throughout the paper, these two polarization configurations are called, respectively, the parallel and cross polarization configurations and are represented in Figure 2a, where the angle θ between the incident light polarization and the crystalline b direction is also defined. Angle-dependent Raman data were collected for every 10° of half-waveplate rotation. The half-waveplate rotate every 10° from 0°-360°, allowing the measurement of the angular dependence of the Raman intensities in both polarization configurations.

UV-Vis-NIR Diffuse Reflectance Spectroscopy: The UV-Vis-NIR diffuse reflectance data were recorded at room temperature using a powdered $BaSO_4$ sample as a standard (100% reflectance) on a PerkinElmer Lamda-950 UV-Vis-NIR spectrophotometer. The scanning wavelength range is from 400 nm to 4000 nm (Figure S10). Absorption (K/S) data were calculated from the following Kubelka-Munk function:[7]

$$F(R) = (1 - R)^2 / (2R) = K/S \quad \text{Eq (1)}$$

where R is the reflectance, K is the absorption, and S is the scattering. In the (K/S) versus

E plot, extrapolating the linear portion of the rising curve to zero gives rise to the onset of absorption.

***Birefringence Tests*:** The birefringence of $(C_6N_2H_{15})Cd(SCN)_3$ and $(C_6N_2H_{16})Cd_2Cl_6 \cdot 2H_2O$ were characterized by using the polarized microscope (NIKON ECLIPSE LV100N POL) equipped with a Berek compensator. Owing to the clear boundary lines of the first-, second- and third-order interference color, the relative error was small enough. The small and transparent $(C_6N_2H_{15})Cd(SCN)_3$ and $(C_6N_2H_{16})Cd_2Cl_6 \cdot 2H_2O$ crystals were chosen to measure, in order to improve the accuracy of the birefringence. The thickness of the selected crystals were measured on the polarized microscope. The formula for calculating the birefringence is listed below:

$$R = |Ne - No| \times T = \Delta n \times T \quad \text{Eq (2)}$$

Here, R represents the optical path difference, Δn means the birefringence, and T is the thickness of the crystal.

***Theoretical Calculations*:** First-principles calculations for $(C_6N_2H_{15})Cd(SCN)_3$ and $(C_6N_2H_{16})Cd_2Cl_6 \cdot 2H_2O$ were carried out with the CASTEP software,[4] a plane-wave pseudopotential package[5] on the basis of the density functional theory (DFT).[6] The exchange-correlation energy was described by the generalized gradient approximation (GGA) scheme of the Perdew-Burke-Ernzerhof (PBE) functional, as implemented in the CASTEP code.[7] Norm-conserving pseudopotentials were employed to simulate the ion-electron interactions for each atomic species with following valence configurations: H $1s^1$, C $2s^22p^2$, N $2s^22p^3$, O $2s^22p^4$, S $3s^22p^4$, and Cd $4d^{10}5s^2$.[8] A kinetic energy cutoff of 830 eV and the Monkhorst-Pack[9] k-point meshes of 3 × 2 × 2 were chosen for the calculation of birefringence, the highest occupied molecular orbitals, the lowest unoccupied molecular orbitals, density of states (DOS), and partial DOS. Based on the calculated band structure, the imaginary part of the dielectric constants can be calculated by the electron transition from the valence bands (VB) to the conduction band (CB). Accordingly, the real part of the dielectric constant (i.e., the refractive

index) was then obtained via a Kramers-Kronig transform of the calculated imaginary part. Subsequently, the refractive indices n and the birefringence Δn were thereby obtained.

Ab initio calculations were conducted by the Gaussian 16 program.[10] The structures used for calculations were fully optimized using wb97xd functional with SDD/aug-cc-pVTZ basis sets. In order to discuss the optical anisotropy of $Cd(SCN)_6$ and $CdCl_5 \cdot H_2O$, the polarizability and polarizability anisotropy of the optimized structures were investigated using wb97xd SDD/aug-cc-pVTZ. The wavefunction analysis was carried out with Multiwfn 3.8 (dev) code,[11] and the isosurface graphs were rendered by the VMD program.[12]

The anisotropy of the polarizability tensor was defined by the static polarizability tensor, according to the following Eq (3).[13] Detailed static polarizability and polarizability anisotropy for different groups were shown in Table S6. Herein, we choose the most commonly used one, a.u., as the unit of the polarizability anisotropy. It is clear that the polarizability is highly anisotropic.

$$\Delta\alpha = \sqrt{[(\alpha_{xx} - \alpha_{yy})^2 + (\alpha_{xx} - \alpha_{zz})^2 + (\alpha_{yy} - \alpha_{zz})^2 + 6(\alpha_{xy}^2 + \alpha_{xz}^2 + \alpha_{yz}^2)]/2} \quad \text{Eq (3)}$$

where α represents the static polarizability tensor, δ represents anisotropy of the polarizability tensor.

Figures

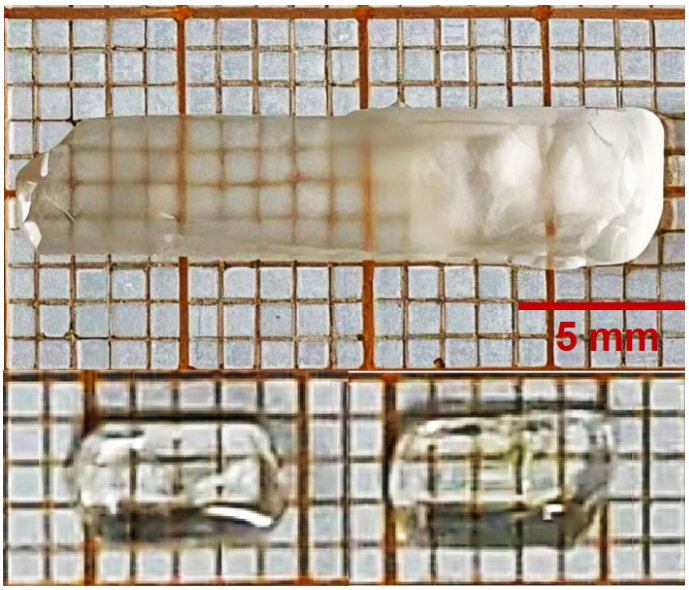

Figure S1. The original single crystals of $(C_6N_2H_{15})Cd(SCN)_3$.

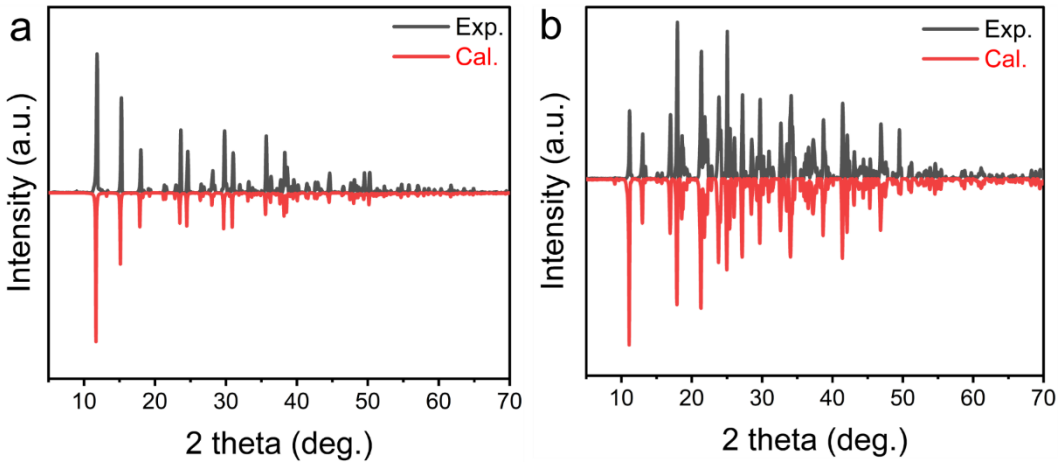

Figure S2. Simulated and experimental PXRD patterns of (a) $(C_6N_2H_{16})Cd_2Cl_6 \cdot 2H_2O$ and (b) $(C_6N_2H_{15})Cd(SCN)_3$.

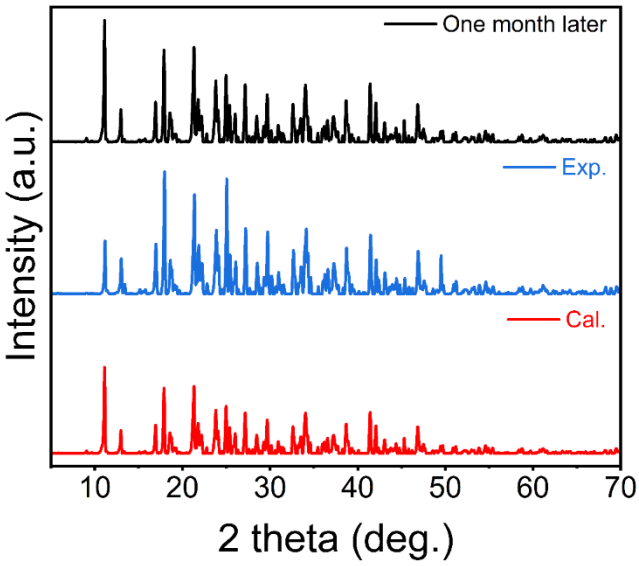

Figure S3. $(C_6N_2H_{15})Cd(SCN)_3$ single crystal exposed to the air at room temperature for one month.

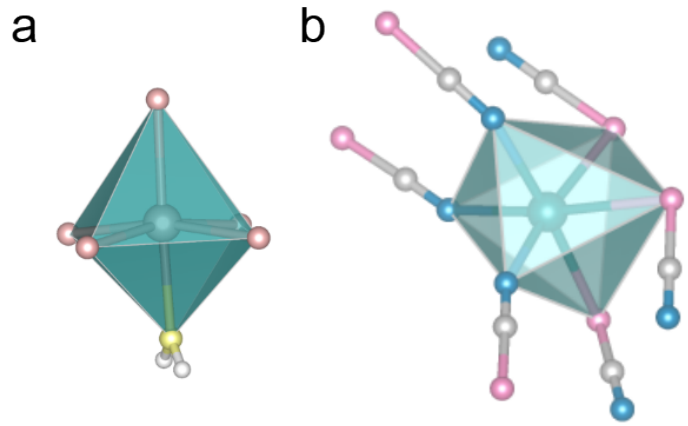

Figure S4. (a) $CdCl_5(H_2O)$ octahedron and (b) $Cd(SCN)_6$ octahedron.

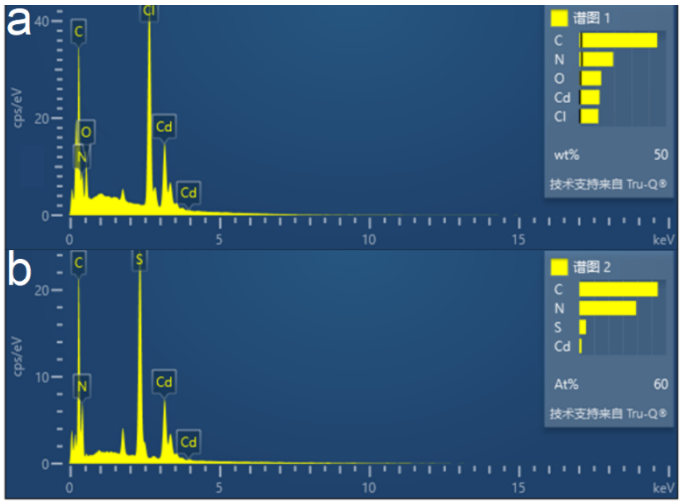

Figure S5. Energy dispersive X-ray spectroscopy result for (a) $(C_6N_2H_{16})Cd_2Cl_6 \cdot 2H_2O$ and (b) $(C_6N_2H_{15})Cd(SCN)_3$.

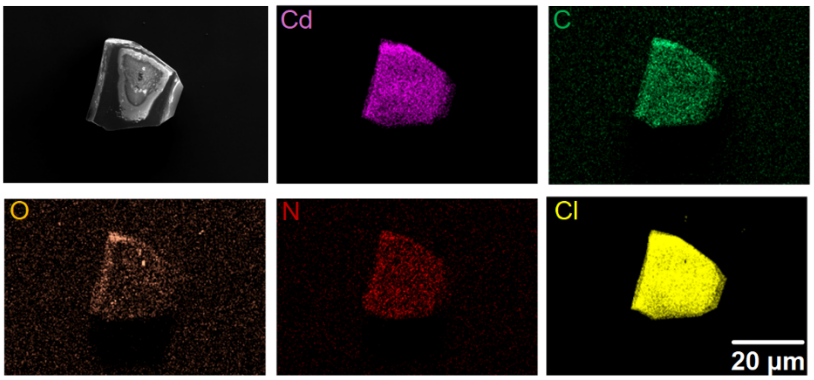

Figure S6. Elements mapping of $(C_6N_2H_{16})Cd_2Cl_6 \cdot 2H_2O$ crystal.

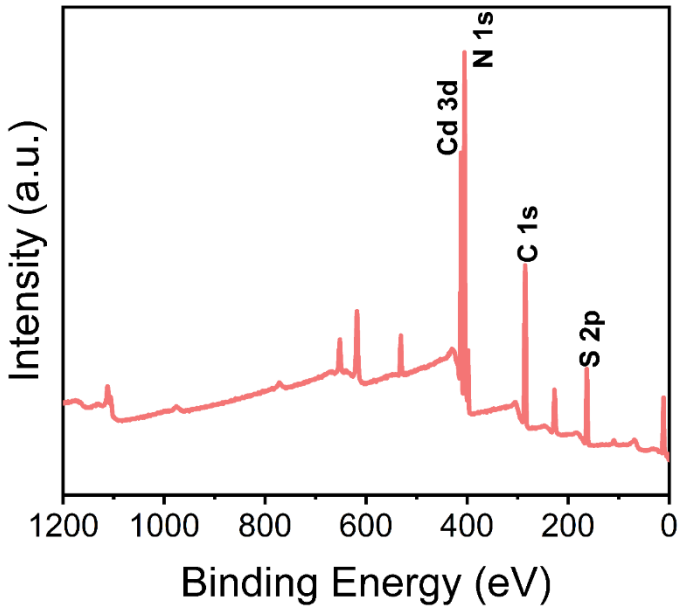

Figure S7. The XPS survey scan of $(C_6N_2H_{15})Cd(SCN)_3$.

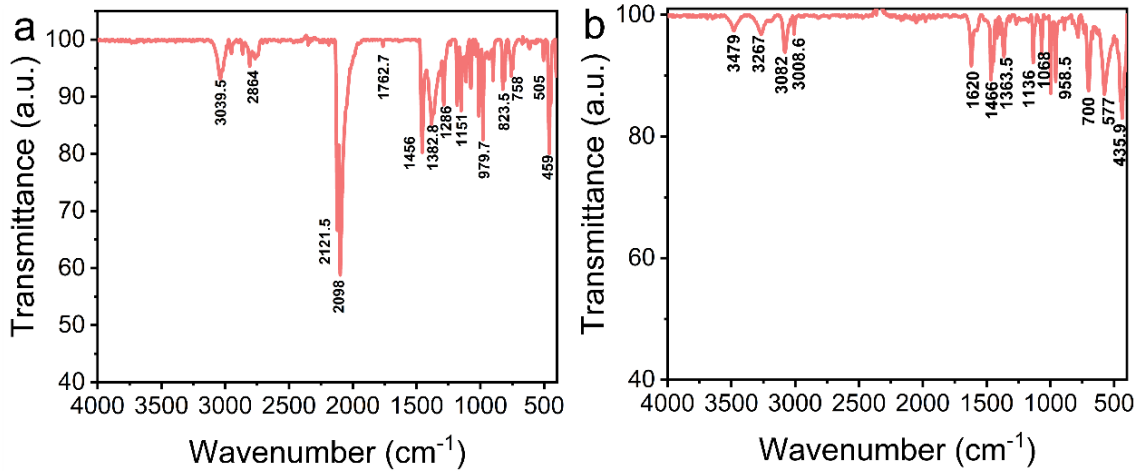

Figure S8. FTIR of (a) $(C_6N_2H_{15})Cd(SCN)_3$ and (b) $(C_6N_2H_{16})Cd_2Cl_6 \cdot 2H_2O$ in the wavenumber of 4000-400 cm^{-1}.

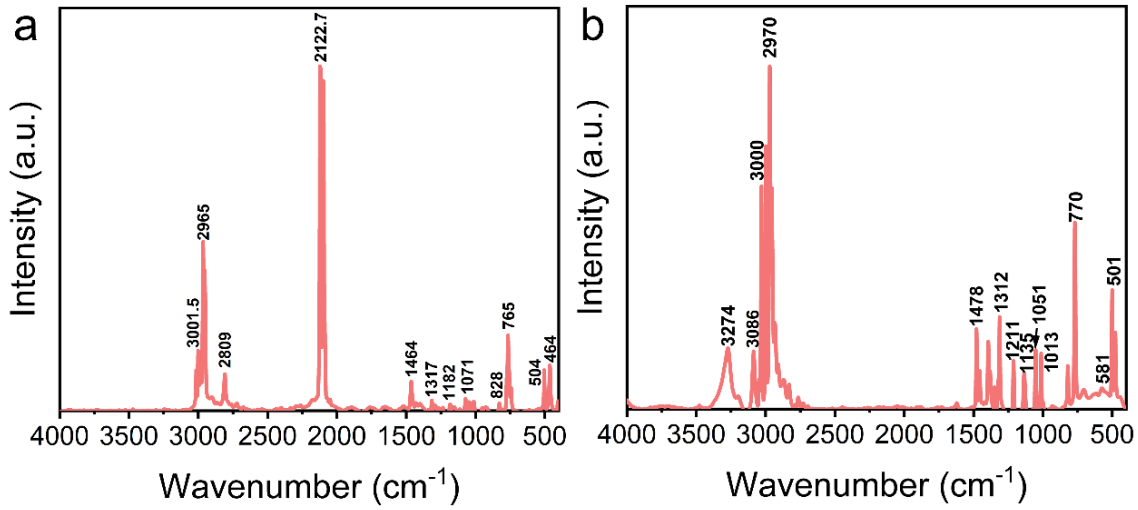

Figure S9. Raman spectroscopy of $(C_6N_2H_{15})Cd(SCN)_3$ and (b) $(C_6N_2H_{16})Cd_2Cl_6{\cdot}2H_2O$ in the wavenumber of 4000-400 cm^{-1}.

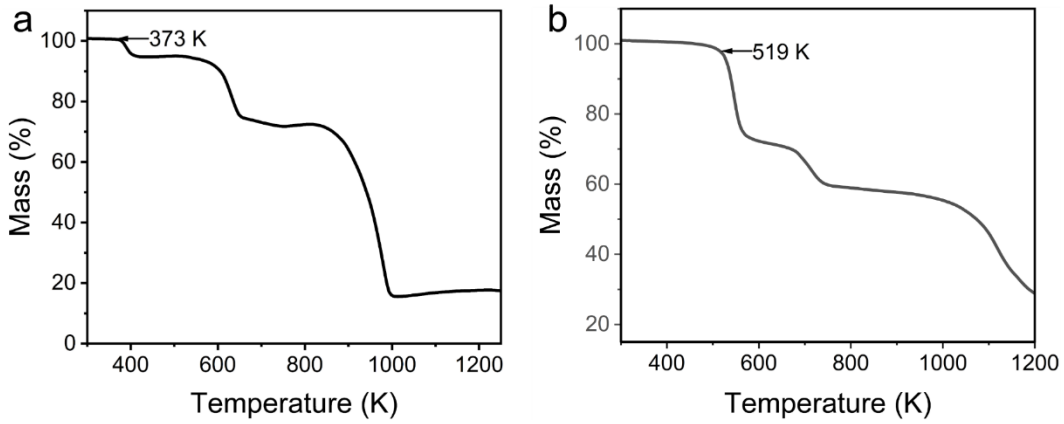

Figure S10. TG curves of (a) $(C_6N_2H_{16})Cd_2Cl_6 \cdot 2H_2O$ and (b) $(C_6N_2H_{15})Cd(SCN)_3$.

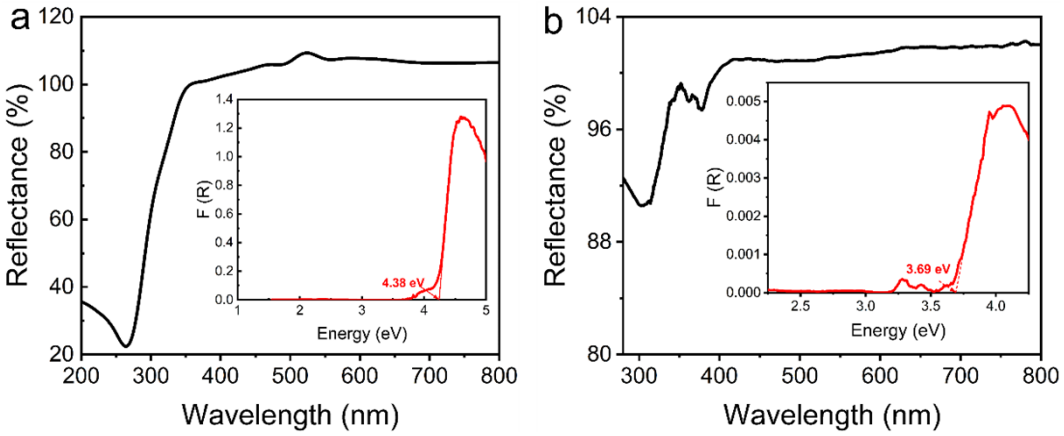

Figure S11. The UV-Vis-NIR diffuse reflectance spectrum of (a) $(C_6N_2H_{16})Cd_2Cl_6 \cdot 2H_2O$ and (b) $(C_6N_2H_{15})Cd(SCN)_3$. The inset indicates the experimental band gap.

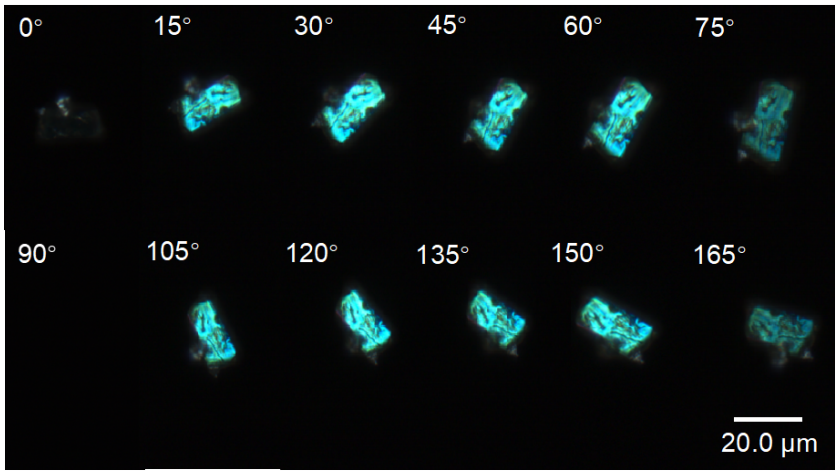

Figure S12. Transmitted images under crossed polarized light in increments of 15° from 0 to 180° for $(C_6N_2H_{15})Cd(SCN)_3$. Scale bar, 20.0 µm.

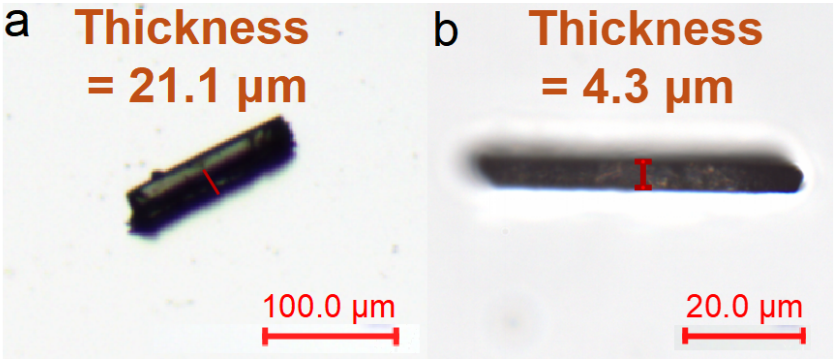

Figure S13. Thickness of (a) $(C_6N_2H_{16})Cd_2Cl_6 \cdot 2H_2O$ and (b) $(C_6N_2H_{15})Cd(SCN)_3$ single crystals for testing birefringence. Scale bar, 100.0 μm (a) and 20.0 μm (b).

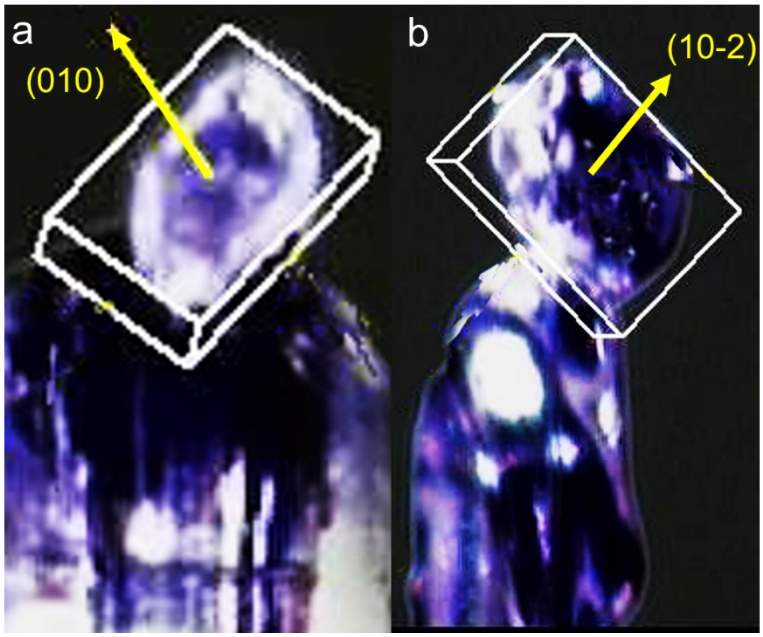

Figure S14. Crystal orientation of (a) $(C_6N_2H_{16})Cd_2Cl_6 \cdot 2H_2O$ and (b) $(C_6N_2H_{15})Cd(SCN)_3$ single crystal used for birefringence test determined by the single-crystal XRD.

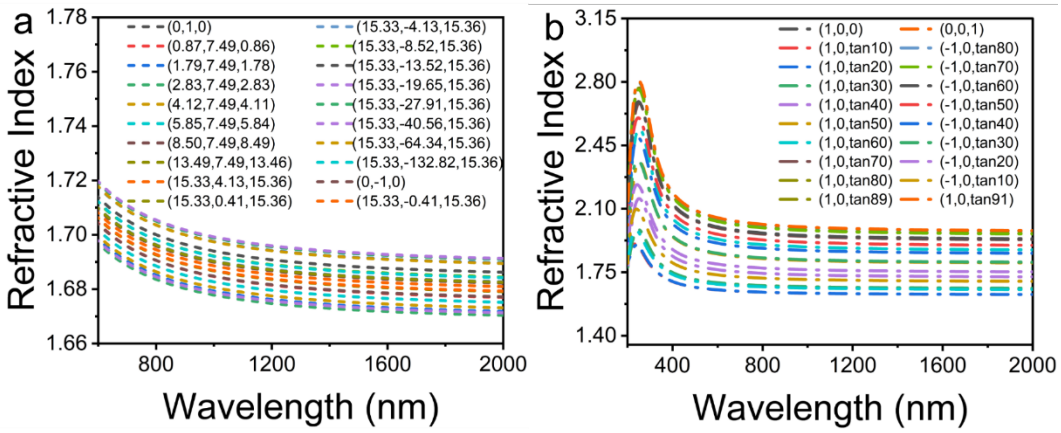

Figure S15. The wavelength-dependent refractive index at angles from 0 to 180° of the (a) (10-2) plane for $(C_6N_2H_{16})Cd_2Cl_6 \cdot 2H_2O$ and (b) the (010) plane for $(C_6N_2H_{15})Cd(SCN)_3$ obtained from theoretical calculations.

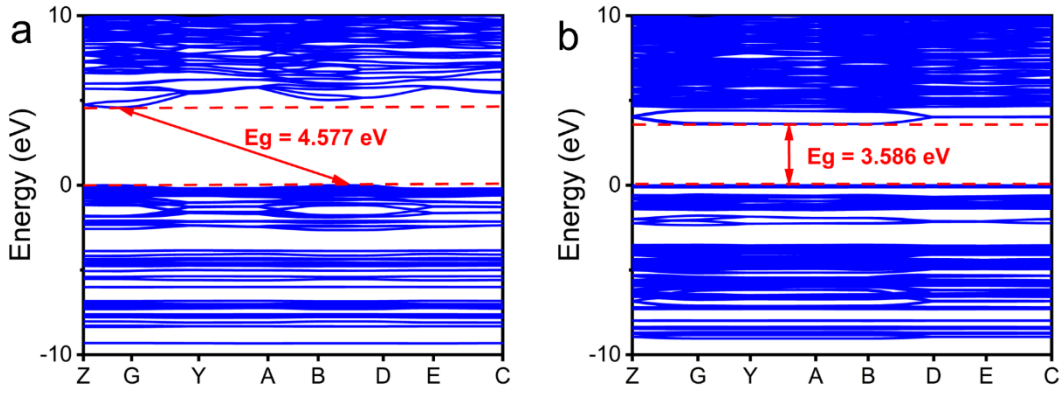

Figure S16. Electronic band structure analyses of (a) $(C_6N_2H_{16})Cd_2Cl_6 \cdot 2H_2O$ and (b) $(C_6N_2H_{15})Cd(SCN)_3$.

Tables

Table S1. Crystal data and structure refinement for $(C_6N_2H_{15})Cd(SCN)_3$ and $(C_6N_2H_{16})Cd_2Cl_6 \cdot 2H_2O$.

	$(C_6N_2H_{15})Cd(SCN)_3$	**$(C_6N_2H_{16})Cd_2Cl_6 \cdot 2H_2O$**
Empirical formula	$C_9H_{15}CdN_5S_3$	$C_3H_{10}CdCl_3NO$
Formula weight	400.83	294.87
Temperature/K	100.15	300.15
Crystal system	monoclinic	monoclinic
space group	$P2_1/c$	$P2_1/c$
a (Å)	10.2074(4)	7.6662(3)
b (Å)	13.7314(4)	7.4855(3)
c (Å)	10.8442(4)	15.3618(7)
α (°)	90	90
β (°)	103.258(4)	99.457(4)
γ (°)	90	90
V (Å^3)	1479.43(9)	869.57(6)
Z	1	4
ρ(calculated) (g cm^{-3})	0.450	2.252
F(000)	199.0	568
Reflections collected	11070	13356
Goodness-of-fit on F^2	1.024	1.044
Final R indexes [I>=2σ (I)][a]	R_1 = 0.0248 wR_2 = 0.0513	R_1 = 0.0221 wR_2 = 0.0438
Final R indexes [all data][a]	R_1 = 0.0327 wR_2 = 0.0534	R_1 = 0.0320 wR_2 = 0.0457

[a] $R_1 = \sum||F_o|-|F_c||/\sum|F_o|$ and $wR_2 = [\sum w(F_o^2-F_c^2)^2/\sum wF_o^4]^{1/2}$ for $F_o^2 > 2\sigma(F_c^2)$.

Table S2. Fractional Atomic Coordinates (× 10^4) and Equivalent Isotropic Displacement Parameters (Å^2 × 10^3) for $(C_6N_2H_{15})Cd(SCN)_3$ and $(C_6N_2H_{16})Cd_2Cl_6 \cdot 2H_2O$.

$(C_6N_2H_{15})Cd(SCN)_3$				
Atom	*x*	*y*	*z*	*U*(eq)
Cd1	2224.9(2)	2808.5(2)	4953.5(2)	14.30(5)
S1	4111.7(6)	1127.6(4)	8947.0(5)	15.89(11)
S2	124.0(6)	1361.2(4)	8238.4(5)	18.81(12)
S3	2385.7(6)	600.6(4)	1356.4(5)	21.32(12)
N1	3836.6(18)	2030.9(13)	6565.7(18)	16.8(4)
N2	758.2(18)	2041.8(14)	5997.3(19)	19.0(4)
N3	2283.4(19)	1579.9(13)	3602.5(18)	18.5(4)
C1	3948(2)	1657.3(15)	7546(2)	13.5(4)
C2	518(2)	1769.4(15)	6932(2)	14.5(4)
C3	2325(2)	1184.8(15)	2674(2)	15.1(4)
N4	7624.6(18)	4051.3(13)	7038.4(18)	17.0(4)
N5	7117.2(18)	3789.7(13)	9522.5(18)	16.2(4)
C4	8110(3)	3713.5(17)	5914(2)	25.0(5)
C5	6491(2)	3431.9(17)	7261(2)	20.6(5)
C6	6015(2)	3797.4(17)	8398(2)	19.8(5)
C7	8180(2)	4440.1(15)	9317(2)	17.9(5)
C8	8731(2)	4086.4(16)	8220(2)	19.1(5)
C9	6635(2)	4088.7(17)	10635(2)	21.6(5)
$(C_6N_2H_{16})Cd_2Cl_6 \cdot 2H_2O$				
Atom	*x*	*y*	*z*	*U*(eq)
Cd1	5356.9(2)	7553.0(2)	28.03(6)	6465.1(2)
Cl2	5350.4(7)	9034.4(7)	8721.2(4)	29.47(12)
Cl3	5722.3(8)	9005.6(8)	6449.7(4)	33.55(13)
Cl4	8689.1(7)	5888.5(9)	7953.5(4)	38.52(14)
O5	2196(2)	6876(2)	7111.6(11)	35.4(4)
N6	1278(2)	6452(3)	5150.5(12)	30.3(4)

C8	-590(3)	6691(3)	5290.1(17)	35.7(6)
C7	1352(3)	5055(4)	4463.8(17)	36.3(6)
C9	2053(4)	8177(4)	4903.7(18)	42.6(6)

[a] U_{eq} is defined as 1/3 of the trace of the orthogonalized U_{ij} tensor.

Table S3. Anisotropic Displacement Parameters ($Å^2 \times 10^3$) for $(C_6N_2H_{15})Cd(SCN)_3$ and $(C_6N_2H_{16})Cd_2Cl_6 \cdot 2H_2O$.

$(C_6N_2H_{15})Cd(SCN)_3$						
Atom	U_{11}	U_{22}	U_{33}	U_{23}	U_{13}	U_{12}
Cd1	18.56(8)	14.58(8)	10.06(8)	-0.34(6)	3.92(5)	0.83(6)
S1	18.7(3)	16.5(3)	12.5(3)	1.0(2)	3.7(2)	0.2(2)
S2	20.7(3)	21.2(3)	14.9(3)	0.4(2)	4.7(2)	-5.8(2)
S3	38.8(3)	14.0(3)	13.1(3)	-0.7(2)	9.9(2)	-0.6(2)
N1	18.5(9)	19.0(9)	13.2(10)	-0.5(8)	4.0(7)	1.7(7)
N2	17.6(9)	23.0(10)	16.1(10)	-1.8(8)	3.0(7)	-2.7(7)
N3	25.3(10)	15.9(9)	14.4(10)	1.8(8)	4.6(8)	2.9(7)
C1	11.2(10)	13.9(10)	15.4(11)	-4.6(9)	3.5(8)	-0.8(8)
C2	10.9(10)	13.3(10)	18.1(11)	-4.7(9)	0.8(8)	-0.6(8)
C3	17.6(11)	13.7(10)	13.9(11)	4.8(9)	3.2(8)	0.5(8)
N4	19.2(9)	14.8(9)	18.1(10)	2.1(7)	6.4(7)	2.5(7)
N5	17.4(9)	16.5(9)	15.0(9)	0.8(7)	4.4(7)	-3.4(7)
C4	32.1(13)	22.6(12)	23.2(13)	0.3(10)	12.3(10)	5.8(10)
C5	16.8(11)	22.6(11)	21.6(12)	-1.5(10)	2.4(9)	-4.1(9)
C6	13.7(10)	24.7(12)	20.2(12)	-2.5(10)	1.8(9)	-4.5(9)
C7	17.5(11)	15.4(10)	18.7(12)	1.0(9)	-0.3(8)	-2.6(8)
C8	15.4(11)	18.6(11)	22.7(12)	3.2(9)	3.2(9)	-0.3(8)
C9	21.9(11)	25.5(12)	16.9(12)	-0.2(10)	3.5(9)	-1.5(9)
$(C_6N_2H_{16})Cd_2Cl_6 \cdot 2H_2O$						
Atom	U_{11}	U_{22}	U_{33}	U_{23}	U_{13}	U_{12}
Cd1	26.23(10)	23.99(9)	2.17(6)	-0.92(7)	32.97(10)	-0.66(7)
Cl2	32.4(3)	28.0(3)	28.6(3)	-0.1(2)	6.6(2)	0.8(2)
Cl3	42.6(3)	28.8(3)	30.6(3)	0.8(2)	9.8(2)	-1.8(2)
Cl4	23.8(3)	44.1(4)	47.1(4)	-1.4(3)	4.3(2)	-2.1(2)

O5	27.3(9)	39.3(10)	39.4(10)	5.6(7)	5.3(7)	-1.6(7)
N6	25.0(9)	40.3(12)	24.3(10)	3.6(8)	0.4(7)	-2.2(8)
C8	27.0(12)	42.2(15)	37.7(14)	-3.4(11)	4.7(9)	1.8(10)
C7	29.7(13)	47.9(16)	33.1(13)	-3.4(11)	10.6(10)	-3.4(11)
C9	40.9(15)	43.6(16)	40.9(15)	3.7(11)	-0.4(11)	12.0(12)

Table S4. Bond Lengths for $(C_6N_2H_{15})Cd(SCN)_3$ and $(C_6N_2H_{16})Cd_2Cl_6 \cdot 2H_2O$.

Selected bond lengths (Å) for $(C_6N_2H_{15})Cd(SCN)_3$			
Cd1–S1[1]	2.8280(6)	N2–C2	1.158(3)
Cd1–S2[1]	2.7435(6)	N3–C3	1.153(3)
Cd–S3[2]	2.6454(6)	N4–C4	1.491(3)
Cd1–N1	2.3627(18)	N4–C5	1.500(3)
Cd1–N2	2.3253(19)	N4–C8	1.502(3)
Cd1–N3	2.2440(19)	N5–C6	1.457(3)
S1–C1	1.658(2)	N5–C7	1.461(3)
S2–C2	1.657(2)	N5–C9	1.462(3)
S3–C3	1.657(2)	C5–C6	1.510(3)
N1–C1	1.162(3)	C7–C8	1.508(3)
Selected bond lengths (Å) for $(C_6N_2H_{16})Cd_2Cl_6 \cdot 2H_2O$			
Cd1–Cl2[1]	2.6622(6)	Cd1–O5	2.4265(16)
Cd1–Cl2	2.6309(6)	N6–C8	1.493(3)
Cd1–Cl3	2.5930(6)	N6–C7	1.493(3)
Cd1–Cl3[1]	2.6148(6)	N6–C9	1.496(3)
Cd1–Cl4	2.5640(6)	C8–C7[2]	1.505(4)

[1]1-X, -1/2+Y, 3/2-Z; [2]-X, 1-Y, 1-Z

Table S5. Bond Angles for $(C_6N_2H_{15})Cd(SCN)_3$ and $(C_6N_2H_{16})Cd_2Cl_6 \cdot 2H_2O$.

Selected bond angles (°) for $(C_6N_2H_{15})Cd(SCN)_3$			
$S2^1$–Cd1–$S1^1$	91.101(17)	C3–S3–Cd1	94.97(7)
$S3^2$–Cd1–$S1^1$	80.646(18)	C1–N1–Cd1	141.39(16)
$S3^2$–Cd1–$S2^1$	88.994(18)	C2–N2–Cd1	149.45(16)
N1–Cd1–$S1^1$	95.67(5)	C3–N3–Cd1	159.31(17)
N1–Cd1–$S2^1$	173.01(5)	N1–C1–S1	179.7(2)
N1–Cd1–$S3^2$	90.39(5)	N2–C2–S2	177.9(2)
N2–Cd1–$S1^1$	173.24(5)	N3–C3–S1	179.0(2)
N2–Cd1–$S2^1$	91.59(5)	C4–N4–C5	111.62(18)
N2–Cd1–$S3^2$	93.20(5)	C4–N4–C8	112.41(18)
N2–Cd1–N1	81.49(6)	C5–N4–C8	109.77(17)
N3–Cd1–$S1^1$	90.80(5)	C6–N5–C7	108.98(17)
N3–Cd1–$S2^1$	90.20(5)	C6–N5–C9	110.31(18)
N3–Cd1–$S3^2$	171.39(5)	C7–N5–C9	110.89(17)
N3–Cd1–N1	91.44(6)	N4–C5–C6	110.30(18)
N3–Cd1–N2	95.39(7)	N5–C6–C5	110.50(18)
C1–S1–$Cd1^2$	101.09(7)	N5–C7–C8	110.35(18)
C2–S2–$Cd1^2$	97.69(7)	N4–C8–C7	109.86(17)
Selected bond angles (°) for $(C_6N_2H_{16})Cd_2Cl_6 \cdot 2H_2O$			
Cl2–Cd1–$Cl2^1$	167.994(9)	O5–Cd1–$Cl2^1$	78.88(4)
$Cl3^1$–Cd1–$Cl2^1$	84.475(18)	O5– Cd1–Cl3	86.25(4)
Cl3–Cd1–$Cl2^1$	92.955(18)	O5– Cd1–$Cl3^1$	81.68(4)
$Cl3^1$–Cd1–Cl2	85.535(18)	O5– Cd1–Cl4	176.70(4)
Cl3–Cd1– $Cl3^1$	94.523(18)	Cd1– Cl2–$Cd1^2$	91.219(17)

Cl4–Cd1–Cl2	167.928(8)	Cd1– Cl2–Cd1[2]	93.146(18)
Cl4–Cd1–Cl2[1]	94.168(19)	C8–N6–C7	109.45(17)
Cl4–Cd1–Cl3[1]	97.820(19)	C8–N6–C9	111.30(17)
Cl4–Cd1–Cl3	98.02(2)	C7–N6–C9	111.26(18)
O5–Cd1–Cl2	94.01(2)	N6–C8–N7[3]	111.70(19)
C1–Cd1–Cl2	89.13(4)	N6–N7–C8[3]	111.63(19)

[1]1-X, -1/2+Y, 3/2-Z; [2]1-X, 1/2+Y, 3/2-Z; [3]-X, 1-Y, 1-Z

Table S6. Static polarizability tensor and corresponding polarizability anisotropy (a.u.) of $Cd(SCN)_6$ and $CdCl_5(H_2O)$.

Groups	Static polarizability (α)						$\Delta\alpha$
	xx	*xy*	*yy*	*xz*	*yz*	*zz*	
$CdCl_5(H_2O)$	210.1	-0.96	212.51	2.00	1.16	207.14	6.37
$Cd(SCN)_6$	536.0	-18.30	399.67	6.27	5.37	372.29	155.8

Table S7. Crystal data and structure refinement for $(C_6N_2H_{15})Cd(SCN)_3$ and $(C_6N_2H_{16})Cd_2Cl_6{\cdot}2H_2O$.

	$(C_6N_2H_{15})Cd(SCN)_3$	**$(C_6N_2H_{16})Cd_2Cl_6{\cdot}2H_2O$**
Empirical formula	$C_9H_{15}CdN_5S_3$	$C_3H_{10}CdCl_3NO$
Formula weight	401.84	294.87
Temperature/K	300.09	300.15
Crystal system	monoclinic	monoclinic
space group	$P2_1/c$	$P2_1/c$
a (Å)	10.28640(8)	7.6662(3)
b (Å)	13.94394(9)	7.4855(3)
c (Å)	10.82874(8)	15.3618(7)
α (°)	90	90
β (°)	102.3951(7)	99.457(4)
γ (°)	90	90
V (Å^3)	1516.993(19)	869.57(6)
Z	4	4
ρ(calculated) (g·cm^{-3})	1.759	2.252
F(000)	800	568
Reflections collected	40315	13356
Goodness-of-fit on F^2	1.053	1.044
Final R indexes [I>=2σ (I)][a]	R_1 = 0.0196 wR_2 = 0.0488	R_1=0.0221 wR_2 = 0.0438
Final R indexes [all data][a]	R_1 = 0.0205 wR_2 = 0.0492	R_1=0.0320 wR_2 = 0.0457

[a]$R_1 = \sum||F_o|-|F_c||/\sum|F_o|$ and $wR_2 = [\sum w(F_o^2-F_c^2)^2/\sum wF_o^4]^{1/2}$ for $F_o^2 > 2\sigma(F_c^2)$.

REFERENCES

(1) Dolomanov, O. V.; Bourhis, L. J.; Gildea, R. J.; Howard, J. A. K.; Puschmann, H. OLEX2: a complete structure solution, refinement and analysis program. *J. Appl. Crystallog.*, 2009, *42*, 339-341.

(2) Sheldrick G. A short history of SHELX. *Acta Crystallogr., Sect. A*, 2008, *64*, 112-122.

(3) Sheldrick G. SHELXT - Integrated space-group and crystal-structure determination. *Acta Crystallogr., Sect. A*, 2015, *71*, 3-8.

(4) Clark S. J.; Segall M. D.; Pickard C. J.; Hasnip P. J.; Probert M. J.; Refson K.; Payne M. C. First principles methods using CASTEP. *Z. Kristallogr.*, 2005, *220*, 567-570.

(5) Payne M. C.; Teter M. P.; Allan D. C.; Arias T. A.; Joannopoulos J. D. Iterative minimization techniques for abinitio total-energy calculations - molecular-dynamics and conjugate gradients. *Rev. Mod. Phys.*, 1992, *64*, 1045-1097.

(6) Kohn W.; Sham L. J. Self-consistent equations including exchange and correlation effects. *Phys. Rev.*, 1965, *140*, 1133-1138.

(7) Perdew J. P.; Burke K.; Ernzerhof M. Generalized gradient approximation made simple. *Phys. Rev. Lett.*, 1996, *77*, 3865-3868.

(8) Rappe A. M.; Rabe K. M.; Kaxiras E.; Joannopoulos J. D. Optimized pseudopotentials. *Phys. Rev. B*, 1990, *41*, 1227-1230.

(9) Monkhorst H. J.; Pack J. D. SPECIAL POINTS FOR BRILLOUIN-ZONE INTEGRATIONS. *Phys. Rev. B*, 1976, *13*, 5188-5192.

(10) Frisch M. J. T., G. W.; Schlegel, H. B.; Scuseria, G. E.; Robb, M. A.; Cheeseman, J. R.; Scalmani, G.; Barone, V.; Mennucci, B.; Petersson, G. A.; Nakatsuji, H.; Caricato, M.; Li, X.; Hratchian, H. P.; Izmaylov, A. F.; Bloino, J.; Zheng, G.; Sonnenberg, J. L.; Hada, M.; Ehara, M.; Toyota, K.; Fukuda, R.; Hasegawa, J.; Ishida, M.; Nakajima, T.; Honda, Y.; Kitao, O.; Nakai, H.; Vreven, T.; Montgomery, J. A., Jr.; Peralta, J. E.; Ogliaro, F.; Bearpark, M.; Heyd, J. J.; Brothers, E.; Kudin, K. N.; Staroverov, V. N.; Kobayashi, R.; Normand, J.; Raghavachari, K.; Rendell, A.; Burant, J. C.; Iyengar, S. S.; Tomasi, J.; Cossi, M.; Rega, N.; Millam, J. M.; Klene, M.; Knox, J. E.; Cross, J. B.; Bakken, V.; Adamo, C.; Jaramillo, J.; Gomperts, R.; Stratmann, R. E.; Yazyev, O.; Austin, A. J.; Cammi, R.; Pomelli, C.; Ochterski, J. W.; Martin, R. L.; Morokuma, K.; Zakrzewski, V. G.; Voth, G. A.; Salvador, P.; Dannenberg, J. J.; Dapprich, S.; Daniels, A. D.; Farkas, Ö.; Foresman, J. B.; Ortiz, J. V.; Cioslowski, J.;

Fox, D. J. *Gaussian 16 Rev. B.01, Wallingford, CT,* 2016.

(11) Lu T.; Chen F. W. Multiwfn: A multifunctional wavefunction analyzer. *J. Comput. Chem.*, 2012, *33*, 580-592.

(12) Humphrey W.; Dalke A.; Schulten K. VMD: Visual molecular dynamics. *J. Mol. Graph.*, 1996, *14*, 33-38.

(13) Alparone A. Linear and nonlinear optical properties of nucleic acid bases. *Chem. Phys.*, 2013, *410*, 90-98.